

Hydrothermal synthesis, characterization and optical properties of $\text{La}_2\text{Sn}_2\text{O}_7:\text{Eu}^{3+}$ micro-octahedra

YANG Jin-yu^{1,2}, SU Yu-chang¹, LIU Xue-ying^{1,3}

1. School of Materials Science and Engineering, Central South University, Changsha 410083, China;
2. School of Chemistry and Materials Science, Guizhou Normal University, Guiyang 550001, China;
3. Department of Science and Technology, Guangxi University of Technology, Liuzhou 545006, China

Received 20 April 2010; accepted 25 June 2010

Abstract: Pyrochlore structure $\text{La}_2\text{Sn}_2\text{O}_7:\text{Eu}^{3+}$ microcrystals with uniform octahedron shape were successfully synthesized via a hydrothermal route at 180 °C for 36 h. The crystal structure, particle size, morphologies, and optical properties of the as-synthesized products were investigated by XRD, TEM, SEM, EDS, FT-IR, Raman spectroscopy and PL. The effects of pH of precursor solution, precursor concentration, reaction temperature, and time were investigated. The results reveal that pH of the precursor solution not only plays an important role in determining the phase of the as-synthesized products, but also has a significant influence on the morphologies of the samples. High-quality and uniform octahedrons with an average size of about 700 nm could be easily obtained at the pH value of 12. The possible formation mechanism of octahedral-like $\text{La}_2\text{Sn}_2\text{O}_7:\text{Eu}^{3+}$ microcrystals was briefly proposed. The photoluminescence spectra show that $\text{La}_2\text{Sn}_2\text{O}_7:\text{Eu}^{3+}$ micro-octahedra display stronger emission in the range of 582–592 nm compared with the samples with other shapes.

Key words: pyrochlore structure; hydrothermal synthesis; growth mechanism; optical properties

1 Introduction

Pyrochlore type complex oxides[1–3] are becoming increasingly important because of their actual and potential applications in the areas of metal-insulator transitions, magnetic frustration/spin ices, magnetoresistance, superconductivity, ferroelectrics, O/F ionic conductivity, mixed conductivity, phosphors, pigments and catalysts. The lanthanum stannates $\text{La}_2\text{Sn}_2\text{O}_7$ have attracted considerable interest recently since they possess excellent chemical and thermal stability, as well as the ability to host rare earth ions in their crystal lattice[4]. The research results revealed that various properties of $\text{La}_2\text{Sn}_2\text{O}_7$ are definitely dependent on their crystal sizes, morphologies, and crystallographic structures[5–7]. Controlled preparation of $\text{La}_2\text{Sn}_2\text{O}_7$ is of great interest and importance. Although various methods, such as conventional solid state approach[8], sol-gel processing[9], co-precipitation route[10], and combustion method[11], have been used to prepare

$\text{La}_2\text{Sn}_2\text{O}_7$, only hydrothermal route has been proved to be a facial approach to fabricate $\text{La}_2\text{Sn}_2\text{O}_7$ nanocrystallites with uniform particle sizes, regular shapes, and pure phases. MOON et al[12] and FU et al[6] have prepared $\text{La}_2\text{Sn}_2\text{O}_7:\text{Eu}^{3+}$ micronanospheres which emitted strong orange-red light under UV excitation. MAO et al[13] have produced $\text{La}_2\text{Sn}_2\text{O}_7$ nanoparticles and observed ionically conducting properties at high temperatures. The flower-like $\text{La}_2\text{Sn}_2\text{O}_7$ nanostructures assembled with nanorods have been fabricated[14]. Nanocubic $\text{La}_2\text{Sn}_2\text{O}_7$ photocatalysts with pyrochlore structure have been successfully synthesized via a one-pot hydrothermal route[5]. However, to the best of our knowledge, by far few reports have been made on the synthesis of $\text{La}_2\text{Sn}_2\text{O}_7$ with octahedron shape by a hydrothermal approach[7].

Herein, a $\text{La}_2\text{Sn}_2\text{O}_7:\text{Eu}^{3+}$ micro-octahedra was fabricated with $\text{La}(\text{NO}_3)_3$, $\text{Eu}(\text{NO}_3)_3$ and SnCl_4 as starting materials via a hydrothermal process without applying any surfactants. The effects of various factors on the formation and morphology of pyrochlore $\text{La}_2\text{Sn}_2\text{O}_7:\text{Eu}^{3+}$ crystals were systematically investigated,

Foundation item: Project (07C26214301746) supported by Innovation Foundation of Ministry of Science and Technology, China; Project (2010GXNSFB013008) supported by Guangxi Natural Science Foundation, China; Project (2009bsxt001) supported by the Graduate Degree Thesis Innovation Foundation of Central South University, China

Corresponding author: SU Yu-chang; Tel/Fax: +86-731-88830785; E-mail: ychsui@mail.csu.edu.cn

DOI: 10.1016/S1003-6326(11)60748-6

and a possible formation mechanism was proposed. In addition, the optical properties of the as-synthesized products were also investigated.

2 Materials and methods

2.1 Materials and preparation of samples

All the reagents in this study were analytically pure and used as-received without further purification. The synthesis of $\text{La}_2\text{Sn}_2\text{O}_7\cdot\text{Eu}^{3+}$ samples via the hydrothermal approach can be described as follows: appropriate amounts of $\text{La}(\text{NO}_3)_3\cdot 6\text{H}_2\text{O}$ and $\text{Eu}(\text{NO}_3)_3\cdot 6\text{H}_2\text{O}$ were dissolved in deionized water to form $\text{La}(\text{NO}_3)_3$ and $\text{Eu}(\text{NO}_3)_3$ solutions, respectively. Then, the required amount of $\text{Eu}(\text{NO}_3)_3$ solution was introduced into the $\text{La}(\text{NO}_3)_3$ solution to form a mixing solution (hereafter referred to $\text{Re}(\text{NO}_3)_3$ solution), and the molar ratio of Eu^{3+} to La^{3+} was fixed to 5:95. The equimolars of $\text{SnCl}_4\cdot 5\text{H}_2\text{O}$ were added in an appropriate amount of $\text{Re}(\text{NO}_3)_3$ solution and stirred for 10 min. Subsequently, the pH of the above solution was adjusted to a desirable value through using 4 mol/L NaOH solution as the mineralizer and the volume was tailored to 64 mL as well while stirring vigorously on a magnetic. The resulting suspension was vigorously stirred for 1 h before it was transferred into a Teflon-lined stainless steel autoclave (80 mL capacity). The autoclave was maintained at a temperature in the range of 160–200 °C for 0–36 h and cooled naturally to ambient temperature. The precipitates were filtered and washed with deionized water repeatedly, and finally dried at 100 °C for 4 h in air.

2.2 Characterization

Crystalline phase was identified by X-ray powder diffraction (XRD) using a Rigaku D/Max 2500 powder diffractometer with Cu K_α radiation ($\lambda=1.5406 \text{ \AA}$). XRD patterns were recorded from 20° to 85° (2θ) with a scan rate of 4°/min. The morphology of the samples was observed by transmission electron microscope (TEM, Philips Tecnai 20 G2 S-TWIN) under an acceleration voltage of 200 kV and combined with energy dispersive X-ray spectroscopy (SEM-EDS, FEI SIRION 200). The Fourier transform infrared (FT-IR) spectrum of the sample was recorded by a Nicolet Avatar 360 IR spectrophotometer. Raman spectrum of the sample was obtained with RFS100/S FT-Raman apparatus from Bruker. The photoluminescence spectra were measured with a Hitachi F-2500 fluorescence spectrometer (resolution: 0.5 nm) at room temperature.

3 Results and discussion

3.1 X-ray diffraction analysis and phase formation

3.1.1 Effect of pH

The crystallinity and phase of the samples were examined by powder XRD. Fig.1(a) shows XRD patterns of as-synthesized samples obtained at different pH values of the reaction solution. It should be noted that three different phases were produced at different pH values. When the pH was 8, all the reflections were indexed to the tetragonal phase SnO_2 (JCPDS 41–1445). By increasing the pH to 9 and 10, a mixture of $\text{La}_2\text{Sn}_2\text{O}_7$ and SnO_2 was obtained. While controlling pH at 11, all the diffraction peaks of the as-synthesized sample can be indexed well to the reference pattern (JCPDS 87–1218), and no impurity peaks can be detected, revealing that the sample possesses a pure cubic pyrochlore structure of $\text{La}_2\text{Sn}_2\text{O}_7$ with space group of $Fd\bar{3}m$ (227). The XRD pattern of the sample prepared at pH 12 is similar with that of the sample obtained at pH 11. However, with increasing the pH to 13, new peaks are developed in the XRD patterns. Those peaks, indicated by square in Fig.1(a), correspond to the hexagonal phase $\text{La}(\text{OH})_3$ (JCPDS 83–2034). As the pH further increases to 14, only reflection peaks corresponding to hexagonal phase $\text{La}(\text{OH})_3$ are found, suggesting that a higher pH favors the formation of $\text{La}(\text{OH})_3$. The EDS spectrum of the sample obtained at pH 12 is shown in Fig.1(b), a small

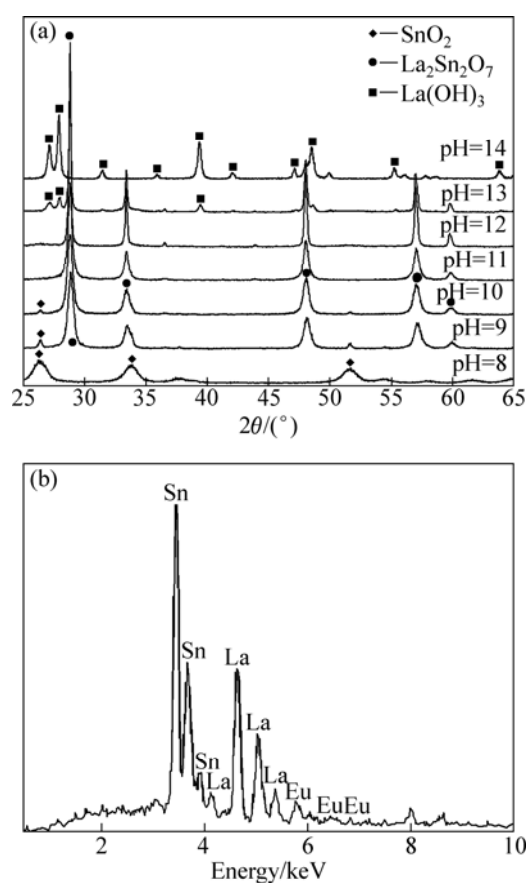


Fig.1 XRD patterns (a) of samples obtained at different pH values and with 78 mmol/L $\text{Re}(\text{NO}_3)_3$ solution under 180 °C for 36 h, and EDS spectrum of sample prepared at pH 12 (b)

quantity of doped Eu^{3+} ions can be found. However, as illustrated by the XRD pattern, the reflection peaks of the sample obtained at pH 12 can be perfectly indexed to a pyrochlore structure of $\text{La}_2\text{Sn}_2\text{O}_7$, suggesting that a small quantity of doped Eu^{3+} ions has a negligible effect on the crystallographic structures of $\text{La}_2\text{Sn}_2\text{O}_7$. On the basis of the above results, it can be concluded that the pH of the reaction solution plays a key role on the formation of phase-pure pyrochlore type $\text{La}_2\text{Sn}_2\text{O}_7:\text{Eu}^{3+}$ crystals.

3.1.2 Effect of precursor concentration

The XRD patterns of the samples synthesized at pH 11 with different precursor concentrations are shown in Fig.2. When the concentration of $\text{Re}(\text{NO}_3)_3$ was 19.5 mmol/L, a mixture of $\text{La}_2\text{Sn}_2\text{O}_7:\text{Eu}^{3+}$ and $\text{La}(\text{OH})_3$ was prepared even though the pH value of the reaction medium was tailored to 11, as shown in Fig.2(a). However, increasing the concentration of $\text{Re}(\text{NO}_3)_3$ to 39 mmol/L or above favors the formation of pure $\text{La}_2\text{Sn}_2\text{O}_7:\text{Eu}^{3+}$ pyrochlore phase (Figs.2(b)–(d)). The results illuminate that the precursor concentration also have effects on the phase composition of products.

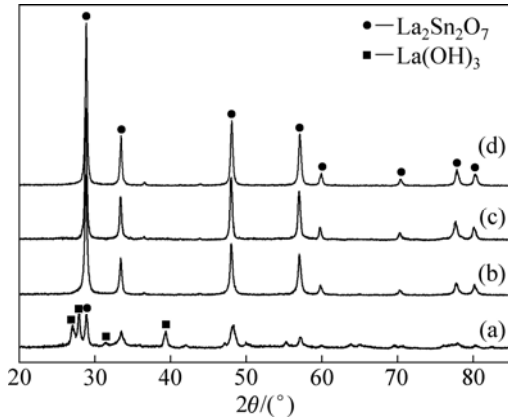
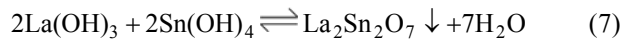
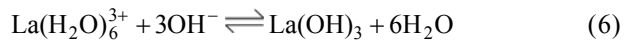
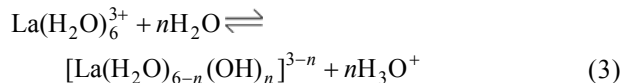
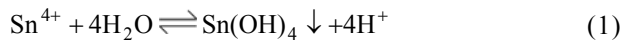


Fig.2 XRD patterns of samples synthesized with various precursor concentrations at pH 11 under 180 °C for 36 h: (a) 19.5 mmol/L $\text{Re}(\text{NO}_3)_3$; (b) 39 mmol/L $\text{Re}(\text{NO}_3)_3$; (c) 78 mmol/L $\text{Re}(\text{NO}_3)_3$; (d) 156 mmol/L $\text{Re}(\text{NO}_3)_3$

3.1.3 Phase formation

Based on the above results, the possible reaction process can be expressed as follows:



In water or weak alkaline solutions ($\text{pH} \leq 8$), due to

the strong hydrolysis effort of Sn^{4+} ions, $\text{Sn}(\text{OH})_4$ colloidal precipitation is formed, as illustrated by Eq.(1) and Eq.(2). Whereas La^{3+} ions exist in the form of $[\text{La}(\text{H}_2\text{O})_{6-n}(\text{OH})_n]^{3-n}$ complexes (Eq.(3)). After hydrothermal process, $\text{Sn}(\text{OH})_4$ colloidal precipitation is converted to SnO_2 crystals (Eq.(4)) while La^{3+} ions still remain in the solution as $[\text{La}(\text{H}_2\text{O})_{6-n}(\text{OH})_n]^{3-n}$ complexes. However, in the strongly basic medium ($\text{pH}=14$), $\text{Sn}(\text{OH})_4$ reacts with OH^- to form soluble $\text{Sn}(\text{OH})_6^{2-}$ species in accordance with Eq.(5). While, La^{3+} ions take on the precipitation of $\text{La}(\text{OH})_3$ via Eq.(6). As $\text{La}(\text{OH})_3$ is very stable under strong basic condition, $\text{La}(\text{OH})_3$ crystals are formed during the hydrothermal process. It is interesting to note that the $\text{La}_2\text{Sn}_2\text{O}_7$ is formed under the medium-strongly alkaline condition ($\text{pH}=11-12$). Under those conditions, La^{3+} and Sn^{4+} ions react with OH^- ions to form $\text{La}(\text{OH})_3$ and $\text{Sn}(\text{OH})_4$ amorphous precipitations, respectively. Then $\text{La}(\text{OH})_3$ and $\text{Sn}(\text{OH})_4$ react with each other to form thermodynamic stable $\text{La}_2\text{Sn}_2\text{O}_7$ crystals through thermal dehydration, as depicted in Eq.(7). The above analysis infers that the coexistence of $\text{La}(\text{OH})_3$ and $\text{Sn}(\text{OH})_4$ was a prerequisite for the formation of $\text{La}_2\text{Sn}_2\text{O}_7$ phase.

As can be seen from Eq.(7), the mole ratio of $\text{La}(\text{OH})_3$ to $\text{Sn}(\text{OH})_4$ is 1:1. From the viewpoint of chemical reaction, $\text{La}(\text{OH})_3$ reacts with equimolar of $\text{Sn}(\text{OH})_4$ to form a single phase $\text{La}_2\text{Sn}_2\text{O}_7$ crystal of pyrochlore structure. The relative excess of $\text{La}(\text{OH})_3$ amorphous precipitation in the system will cause a mixture of $\text{La}_2\text{Sn}_2\text{O}_7$ and $\text{La}(\text{OH})_3$ as product after hydrothermal treatment. Conversely, when $\text{Sn}(\text{OH})_4$ precursor is plentiful and there is a relative shortage of $\text{La}(\text{OH})_3$, the product with mixed phases of $\text{La}_2\text{Sn}_2\text{O}_7$ and SnO_2 will be obtained. It can be inferred that the mole ratio (R) of $\text{La}(\text{OH})_3$ to $\text{Sn}(\text{OH})_4$ in precursor solution is a key factor for the phase composition of product. R can be calculated via the following equation which is derived from Eq.(1), Eq.(5) and Eq.(6)[15]:

$$R = \frac{c_4[\text{OH}^-]^4 - K_{\text{sp1}}[\text{OH}^-]}{c_2[\text{OH}^-]^4 - K_{\text{sp2}} - K[\text{OH}^-]^6} \quad (8)$$

where c_1 and c_2 are the concentrations of $\text{Re}(\text{NO}_3)_3$ and SnCl_4 , respectively; K_{sp1} and K_{sp2} are the solubility products of $\text{Re}(\text{OH})_3$ and $\text{Sn}(\text{OH})_4$, respectively; and K is the equilibrium constant of Eq.(5).

As inferred by Eq.(8), R depends on the concentration of the starting materials and the pH of reaction solution. The calculated values of R under different conditions are listed in Table 1. Based on the calculated values of R under normal state conditions, the phase compositions of products were estimated according to the chemical equilibrium principles and the detection limit of XRD, as shown in Table 1. There is deviation between the estimated phase compositions to

the actual phase compositions since the calculated R is obtained under the normal state. Compared with the experimental results, a similar trend in the change of phases with pH value and precursor concentration is observed from the estimated results, as shown in Table 1. The above results demonstrate unambiguously that the mole ratio of $\text{La}(\text{OH})_3$ to $\text{Sn}(\text{OH})_4$ in precursor solution plays a crucial role in forming the single-phase $\text{La}_2\text{Sn}_2\text{O}_7$.

Table 1 R and phase compositions at different pH and concentrations

pH	$c(\text{Re}(\text{NO}_3)_3)/$ ($\text{mmol}\cdot\text{L}^{-1}$)	R^*	Composition	
			Measured phase	Estimated phase
8	78.0	0	SnO_2	SnO_2
9	78.0	0.97	$\text{La}_2\text{Sn}_2\text{O}_7\cdot\text{Eu}^{3+}+\text{SnO}_2$	$\text{La}_2\text{Sn}_2\text{O}_7\cdot\text{Eu}^{3+}$
10	78.0	1.00	$\text{La}_2\text{Sn}_2\text{O}_7\cdot\text{Eu}^{3+}+\text{SnO}_2$	$\text{La}_2\text{Sn}_2\text{O}_7\cdot\text{Eu}^{3+}$
11	78.0	1.04	$\text{La}_2\text{Sn}_2\text{O}_7\cdot\text{Eu}^{3+}$	$\text{La}_2\text{Sn}_2\text{O}_7\cdot\text{Eu}^{3+}$
12	78.0	$+\infty$	$\text{La}_2\text{Sn}_2\text{O}_7\cdot\text{Eu}^{3+}$	$\text{La}(\text{OH})_3$
13	78.0	$+\infty$	$\text{La}_2\text{Sn}_2\text{O}_7\cdot\text{Eu}^{3+}+\text{La}(\text{OH})_3$	$\text{La}(\text{OH})_3$
14	78.0	$+\infty$	$\text{La}(\text{OH})_3$	$\text{La}(\text{OH})_3$
11	19.5	1.19	$\text{La}_2\text{Sn}_2\text{O}_7\cdot\text{Eu}^{3+}+$ $\text{La}(\text{OH})_3$	$\text{La}_2\text{Sn}_2\text{O}_7\cdot\text{Eu}^{3+}+$ $\text{La}(\text{OH})_3$
11	39.0	1.08	$\text{La}_2\text{Sn}_2\text{O}_7\cdot\text{Eu}^{3+}$	$\text{La}_2\text{Sn}_2\text{O}_7\cdot\text{Eu}^{3+}$
11	156.0	1.02	$\text{La}_2\text{Sn}_2\text{O}_7\cdot\text{Eu}^{3+}$	$\text{La}_2\text{Sn}_2\text{O}_7\cdot\text{Eu}^{3+}$

R^* is the mole ratio of $\text{La}(\text{OH})_3$ to $\text{Sn}(\text{OH})_4$ in reaction solution, calculated from the solubility equilibrium theory under normal state conditions.

3.1.4 Effect of reaction temperature

The effect of the reaction temperature on the formation of crystalline $\text{La}_2\text{Sn}_2\text{O}_7$ is illuminated by XRD patterns in Fig.3. The pH, the concentration of $\text{Re}(\text{NO}_3)_3$, and time were maintained at 11, 39 mmol/L, and 18 h, respectively. The XRD pattern shows that the sample obtained at 160 °C is a mixture of $\text{La}(\text{OH})_3$ crystals (JCPDS 83–2034) and amorphous SnO_2 . The diffraction peaks of the sample obtained at 180 °C are indexed to $\text{La}_2\text{Sn}_2\text{O}_7$ phase (JCPDS 87–1218), and no impurity peaks are detected. These results confirmed that

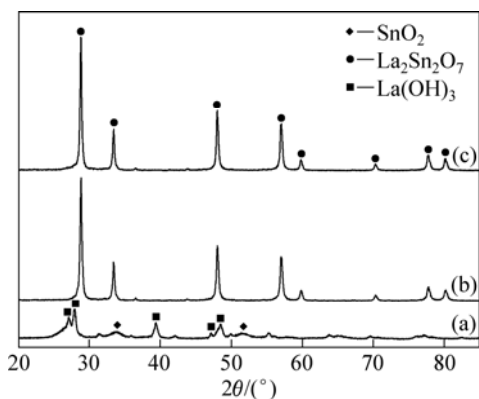


Fig.3 XRD patterns of samples produced at pH 11 with 39 mmol/L $\text{Re}(\text{NO}_3)_3$ solution under different temperatures for 18 h: (a) 160 °C; (b) 180 °C; (c) 200 °C

$\text{La}_2\text{Sn}_2\text{O}_7$ phase began to appear in the temperature range of 160–180 °C and was formed completely at 180 °C. Elevating reaction temperature to 200 °C causes an increase of diffraction peak intensity originated from the improved crystallinity.

3.1.5 Effect of reaction time

Fig.4 shows the XRD patterns of the time-series samples synthesized at pH 11 with 39 mmol/L $\text{Re}(\text{NO}_3)_3$ solution under 180 °C. No diffraction peak appears for the sample prepared by precipitation, indicating that the sample is amorphous. Increasing time of hydrothermal treatment to 2 h reveals significant differences in the XRD pattern. The diffraction peak of $\text{La}_2\text{Sn}_2\text{O}_7$ (222) plane appeared at 28.79° although the major diffraction peaks corresponding to the $\text{La}(\text{OH})_3$ could be observed. From a kinetic viewpoint, this suggests precipitation of $\text{La}(\text{OH})_3$ prior to $\text{La}_2\text{Sn}_2\text{O}_7$. When the reaction was carried out for 8 h or more, only $\text{La}_2\text{Sn}_2\text{O}_7$ could be detected by XRD, indicating that $\text{La}(\text{OH})_3$ and SnO_2 had been transformed completely into $\text{La}_2\text{Sn}_2\text{O}_7$. With increasing the reaction time, the peak-width decreases and the peak intensity increases while the peaks position kept constant, revealing that the crystal size increases and the crystallinity of $\text{La}_2\text{Sn}_2\text{O}_7\cdot\text{Eu}^{3+}$ becomes better.

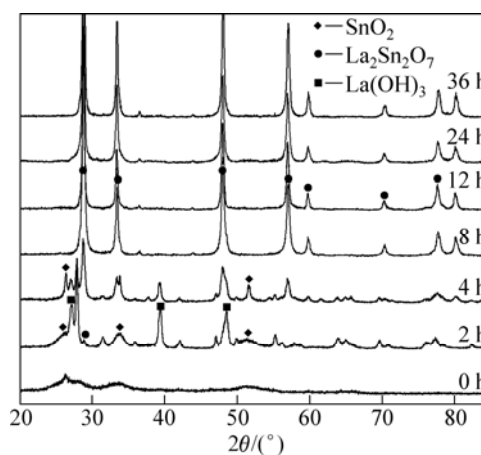


Fig.4 XRD patterns of samples prepared at pH 11 with 39 mmol/L $\text{Re}(\text{NO}_3)_3$ solution under 180 °C for different hydrothermal treatment time

The above results demonstrate that a longer hydrothermal reaction time at a higher temperature favors the formation and crystallization of the thermodynamically stable $\text{La}_2\text{Sn}_2\text{O}_7\cdot\text{Eu}^{3+}$.

3.2 Morphology and growth mechanism

3.2.1 Electron microscopy

To further explore the effects of the pH of precursor solutions, reaction time, and precursor concentration on sizes and shapes of the samples, SEM and TEM were used to characterize the as-synthesized $\text{La}_2\text{Sn}_2\text{O}_7\cdot\text{Eu}^{3+}$ crystals. SEM and TEM images are shown in Fig.5.

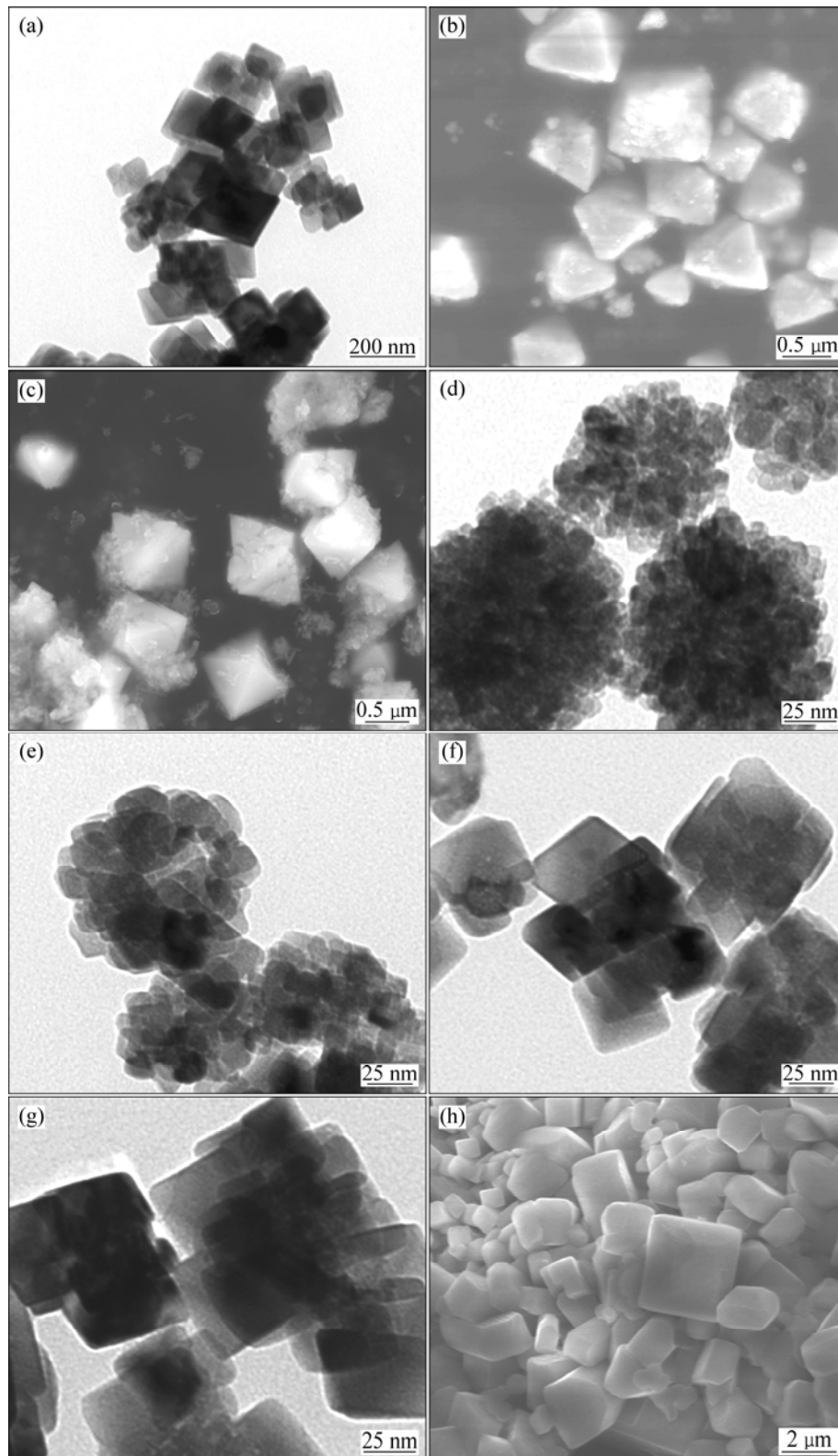


Fig.5 TEM and SEM images of as-synthesized samples at 180 °C with different pH values, $\text{Re}(\text{NO}_3)_3$ concentration, and hydrothermal treatment time: (a) TEM, pH 11, 78 mmol/L, 36 h; (b) SEM, pH 12, 78 mmol/L, 36 h; (c) SEM, pH 13, 78 mmol/L, 36 h; (d) TEM, pH 11, 39 mmol/L, 8 h; (e) TEM, pH 11, 39 mmol/L, 12 h; (f) TEM, pH 11, 39 mmol/L, 24 h; (g) TEM, pH 11, 39 mmol/L, 36 h; (h) SEM, pH 11, 156 mmol/L, 36 h

The TEM image of $\text{La}_2\text{Sn}_2\text{O}_7\cdot\text{Eu}^{3+}$ derived from a pH 11 precursor solution in the presence of 78 mmol/L

$\text{Re}(\text{NO}_3)_3$ solution at 180 °C for 36 h is shown in Fig.5(a). It is shown that the sample exhibits a mixture of

frustum of pyramids-like crystals and irregular crystals with an average diameter of about 150 nm. However, when the pH was tailored to 12 while other parameters kept constant, the morphology of products dramatically changes to perfect 3D octahedron with an average size of 700 nm, as shown in Fig.5(b). Once the pH value was modulated at 13, the majority of products take on the shape of octahedron (Fig.5(c)). When the pH and the concentration of $\text{Re}(\text{NO}_3)_3$ were maintained at 11 and 39 mmol/L, respectively, it was clearly shown that the sample obtained at 8 h displays irregular nanospheres shape with an average diameter of about 90 nm (Fig.5(d)). Fig.5(d) also demonstrates that the sphere-like structure was formed by the assembly of nanoparticles with size of around 12 nm. With increasing the hydrothermal treatment time to 12 h, the TEM image shown in Fig.5(e) displays that the sample has similar morphology to the sample obtained at 8 h, except that the spheres are assembled by well-crystalline nanocrystals with size of about 16 nm. Fig.5(f) shows that the sample obtained by hydrothermal treatment for 24 h possesses irregular frustum of pyramids-like morphology with size of about 48 nm. When the time of hydrothermal treatment was prolonged to 36 h, the as-synthesized $\text{La}_2\text{Sn}_2\text{O}_7:\text{Eu}^{3+}$ nanocrystals with similar morphology to the sample obtained at 24 h were observed in Fig.5(g). The average size of crystals is about 50 nm. The SEM image of sample obtained from a pH 11 precursor solution in the presence of 156 mmol/L $\text{Re}(\text{NO}_3)_3$ at 180 °C for 36 h is shown in Fig.5(h). It is obvious that the sample presents irregular polyhedral shape with wide size of 700–3 000 nm.

It can be inferred from those TEM and SEM images that the size of products is mostly determined by both the precursor concentration and the pH of reaction solutions, even though a longer hydrothermal reaction time favors the formation of well-crystallized products. Especially, the pH values of the reaction solutions do have significant effects on the fabrication of $\text{La}_2\text{Sn}_2\text{O}_7:\text{Eu}^{3+}$ with octahedral morphology.

3.2.2 Growth mechanism

Generally, chemical growth of materials inevitably involves the process of precipitation of a solid phase from solution which basically consists of a nucleation step followed by particle growth stages. The surface energy of the crystallographic faces of the seeds strongly influences the anisotropic growth patterns of the crystals. And it can be altered by controlling the concentration of OH^- ions that are adsorbed onto surfaces of the growing crystallites[16]. pH has been widely used to stabilize certain faces of nanocrystals by selective adhesion to fabricate crystals with cube-like, sheet-like, and rod-like shapes[17–19]. In the present case, three-dimensional clusters with critical sizes were first formed as $\text{La}_2\text{Sn}_2\text{O}_7$

nuclei and then further grew into crystallites. Under an basic condition (pH=11), the lone electron pairs in O atoms could strongly interact with the surface of $\text{La}_2\text{Sn}_2\text{O}_7$ nuclei and preferably adhere to some special crystalline faces due to the larger atomic densities of the crystallite faces. However, when the pH of precursor solution was increased to a higher value (pH \geq 12), a large amount of OH^- ions were presented in solution, and each face of the crystallite has almost the same probability to generate active sites, leading to the homogeneous absorption of OH^- ions. As a capping agent, the adsorbed OH^- generated the shielding effect to slow the growth of the adsorbed crystal faces, leading to the formation of frustum of pyramids-like or octahedral-like $\text{La}_2\text{Sn}_2\text{O}_7:\text{Eu}^{3+}$ crystals.

On the basis of the above analysis results, a schematic illustration of the formation mechanism of $\text{La}_2\text{Sn}_2\text{O}_7:\text{Eu}^{3+}$ is proposed in Fig.6.

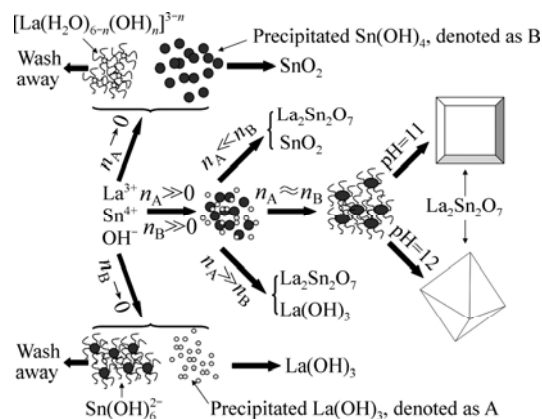


Fig.6 Schematic illustration of formation mechanism of samples with different phases and shapes (n denotes the number of precipitates)

3.3 Optical properties

3.3.1 FT-IR and Raman analysis

Fig.7(a) shows the FT-IR spectrum of the octahedral $\text{La}_2\text{Sn}_2\text{O}_7:\text{Eu}^{3+}$ crystals. In the range of 1 300–400 cm^{-1} , only two broad bands are clearly observed. The absorption band at 599 cm^{-1} corresponds to the Sn—O stretching vibration in the octahedral SnO_6 and the strong stretching vibration of La—O is located at 418 cm^{-1} . The FT-IR spectrum of the octahedral $\text{La}_2\text{Sn}_2\text{O}_7:\text{Eu}^{3+}$ crystals shows a small blue (or red) shift as compared with other reports[6, 13], it may result from the differences in the morphology, size, and Eu^{3+} doping.

According to group theoretical analysis[20], the pyrochlore structure possesses six Raman active modes ($\Gamma=A_{1g}+E_g+4F_{2g}$). The observed Raman spectrum of the octahedral $\text{La}_2\text{Sn}_2\text{O}_7:\text{Eu}^{3+}$ crystals is presented in Fig.7(b). The modes at 300, 340, 398, 501, 550, and 615 cm^{-1} can be assigned to F_{2g} , E_g , F_{2g} , A_{1g} , F_{2g} , and F_{2g} , respectively. It should be noted that an obvious peak

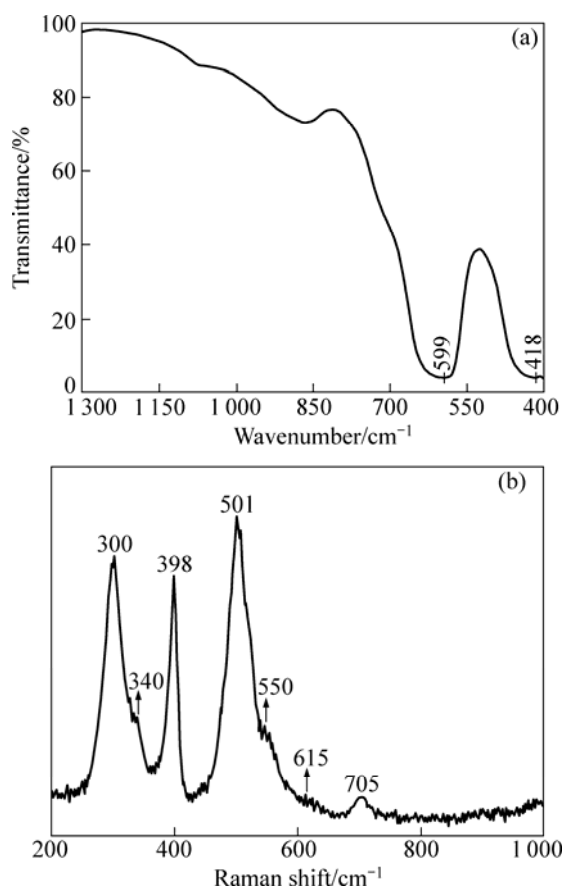


Fig.7 FT-IR spectrum (a) and Raman spectrum (b) of octahedral $\text{La}_2\text{Sn}_2\text{O}_7:\text{Eu}^{3+}$ microcrystals

located at 705 cm^{-1} appears in the Raman spectrum, which corresponds to the distortion of the SnO_6 octahedral local structure[21]. A similar peak was also observed in other pyrochlore structures[22–23].

3.3.2 Photoluminescence properties

The luminescence characteristics of $\text{La}_2\text{Sn}_2\text{O}_7:\text{Eu}^{3+}$ crystals with different shapes were explored, as shown in Fig.8. Under the excitation of 270 nm, the emission spectra of the irregular nanosphere-like, frustum of pyramid-like, and octahedral-like $\text{La}_2\text{Sn}_2\text{O}_7:\text{Eu}^{3+}$ nano-/micro-structure are denoted as a, b, and c in Fig.8, respectively. All samples exhibit a similar orange-red luminescence. The strongest emission peak at 582–592 nm is originated from the magnetic dipole transition $^5\text{D}_0-^7\text{F}_1$ of Eu^{3+} , while the stronger peak line at 616 nm can be assigned to the electric dipole transition of $^5\text{D}_0-^7\text{F}_2$. The other peaks correspond to the transitions from $^5\text{D}_0$ level to $^7\text{F}_J$ ($J=0, 1, 2, 3$) levels of Eu^{3+} activators, as shown in Fig.8. The emission spectra of the three samples are similar in shape and differ in the band intensity. Generally, the fluorescence intensity ratio of $^5\text{D}_0-^7\text{F}_2$ to $^5\text{D}_0-^7\text{F}_1$, called the asymmetry ratio, depends strongly on the local symmetry of Eu^{3+} ions, and a higher symmetry of the crystals field around Eu^{3+} ions will result in a lower asymmetry ratio. La^{3+} ion is located at

the site with D_{3d} symmetry in $\text{La}_2\text{Sn}_2\text{O}_7$ lattice. Due to the charge and ionic radii, Eu^{3+} will prefer to substitute La^{3+} rather than Sn^{4+} in the $\text{La}_2\text{Sn}_2\text{O}_7$ matrix. The enhanced and sharpened emissions $^5\text{D}_0-^7\text{F}_1$ of Eu^{3+} in the $\text{La}_2\text{Sn}_2\text{O}_7$ host crystals could be reasonably explained by the allowed magnetic dipole transition due to the presence of an inversion center. The asymmetry ratios of the irregular nanosphere-like, frustum of pyramid-like, and octahedral-like $\text{La}_2\text{Sn}_2\text{O}_7:\text{Eu}^{3+}$ are 0.450, 0.395, and 0.301, respectively. The lower asymmetry ratio of the octahedral-like $\text{La}_2\text{Sn}_2\text{O}_7:\text{Eu}^{3+}$ compared with the irregular nanospheres can be explained by the increase of local symmetry of Eu^{3+} ions which may be caused by the oriented growth of the samples. As reported in the previous works, the dipole field was not only influenced by the typical dimensions and dielectric constants of the hosts but also their shape[24–26]. The octahedral-like $\text{La}_2\text{Sn}_2\text{O}_7:\text{Eu}^{3+}$ has higher symmetry shape, and less Eu^{3+} ions occur on the surface compared with the other samples, leading to higher symmetry of dipole field surrounding the Eu^{3+} ions and stronger emission intensity. Furthermore, for the irregular nanosphere-like $\text{La}_2\text{Sn}_2\text{O}_7:\text{Eu}^{3+}$, three lines in the emission spectrum at 587, 594, and 601 nm which assign to $^5\text{D}_0-^7\text{F}_1$ transition can be observed, indicating that a proportion of Eu^{3+} ions was not located in the D_{3d} symmetry site, which may be resulted from the weak crystallinity[27–28]. It was reported the microstructure and size of materials could influence luminescence of phosphor[29–31], which is in good agreement with our results. In our case, the octahedral-like $\text{La}_2\text{Sn}_2\text{O}_7:\text{Eu}^{3+}$ has more regular shape, higher crystallinity, and larger size compared with the other samples, resulting in the less existence of OH^- groups, Eu^{3+} ions, and defects on the surface. It is well known that the excited state of the Eu^{3+} ions can decay

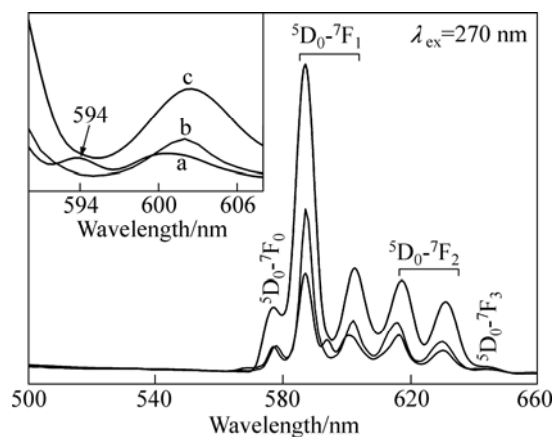


Fig.8 Room-temperature emission spectra of nanosphere-like, frustum of pyramid-like, and 3D octahedron-like $\text{La}_2\text{Sn}_2\text{O}_7:\text{Eu}^{3+}$ nano/microcrystals obtained at $180\text{ }^\circ\text{C}$ with different conditions: (a) pH 11, 39 mmol/L, 8 h; (b) pH 11, 78 mmol/L, 36 h; (c) pH 12, 78 mmol/L, 36 h

nonradiatively by the OH⁻ group vibrations of La/Sn-OH linkages adhered on the surface and the excitation energy can be dissipated through cross-relaxation or quenching by defect sites. The less OH⁻ and defects on the surface, the more intense PL spectrum will be achieved. The results reveal that the shape anisotropy affects the intensity and profile of emission spectra.

4 Conclusions

1) The pyrochlore type La₂Sn₂O₇:Eu³⁺ nano-/micro-crystals were successfully synthesized via a hydrothermal route.

2) The possible formation mechanism of octahedral-like La₂Sn₂O₇:Eu³⁺ with pyrochlore structure was proposed. It is found that the existence of La(OH)₃ and Sn(OH)₄ in the precursor solution is a prerequisite for the formation of La₂Sn₂O₇ phase and the pH value of the reaction solution plays a key role in the fabrication of La₂Sn₂O₇:Eu³⁺ with octahedral morphology.

3) The octahedral-like La₂Sn₂O₇:Eu³⁺ displays improved luminescence than other La₂Sn₂O₇:Eu³⁺ crystals, which would be a promising reddish phosphor for applications in lamps and displays.

References

- [1] SICKAFUS K E, MINERVINI L, GRIMES R W, VALDEZ J A, ISHIMARU M, LI F, MCCLELLAN K J, HARTMANN T. Radiation tolerance of complex oxides [J]. *Science*, 2000, 289: 748–751.
- [2] REN Qing-li, LUO Qiang, CHEN Shou-tian. Optimization of dielectric constant temperature coefficient of pyrochlores containing bismuth [J]. *Transactions of Nonferrous Metals Society of China*, 2005, 15(2): 252–256.
- [3] XUE Ya-hong, LIU Rui-quan, WANG Ji-de, LI Zhi-jie. Structure and ionic conductivities of oxides with a pyrochlore-type structure [J]. *Progress in Chemistry*, 2005, 17(4): 672–677. (in Chinese).
- [4] ALEMI A, KALAN R E. Preparation and characterization of neodymium tin oxide pyrochlore nanocrystals by the hydrothermal method [J]. *Radiation Effects and Defects in Solids*, 2008, 163(3): 229–236.
- [5] ZENG Jia, WANG Hao, ZHANG Yong-cai, ZHU Man-kang, YAN Hui. Hydrothermal synthesis and photocatalytic properties of pyrochlore La₂Sn₂O₇ nanocubes [J]. *Journal of Physical Chemistry C*, 2007, 111(32): 11879–11887.
- [6] FU Z L, YANG H K, MOON B K, CHOI B C, JEONG J H. La₂Sn₂O₇:Eu³⁺ micronanospheres: Hydrothermal synthesis and luminescent properties [J]. *Crystal Growth and Design*, 2009, 9(1): 616–621.
- [7] YANG Jin-yu, SU Yu-chang. Novel 3D octahedral La₂Sn₂O₇:Eu³⁺ microcrystals: Hydrothermal synthesis and photoluminescence properties [J]. *Materials Letters*, 2010, 64(3): 313–316.
- [8] LIAN J, HELEAN K B, KENNEDY B J, WANG L M, NAVROTSKY A, EWING R C. Effect of structure and thermodynamic stability on the response of lanthanide stannate-pyrochlores to ion beam irradiation [J]. *Journal of Physical Chemistry B*, 2006, 110(5): 2343–2350.
- [9] CHENG Hua, WANG Li-ping, LU Zhou-guang. A general aqueous sol-gel route to Ln₂Sn₂O₇ nanocrystals [J]. *Nanotechnology*, 2008, 19(2): 025706.
- [10] WANG Shu-mei, LU Meng-kai, ZHOU Guang-jun, ZHOU Yuan-yuan, ZHANG Hai-ping, WANG Shu-fen, YANG Zhong-sen. Synthesis and luminescence properties of La_{2-x}RE_xSn₂O₇ (RE=Eu and Dy) phosphor nanoparticles [J]. *Materials Science and Engineering B*, 2006, 133(1–3): 231–234.
- [11] WANG Shu-mei, XIU Zhi-liang, LU Meng-kai, ZHANG Ai-yu, ZHOU Yuan-yuan, YANG Zhong-sen. Combustion synthesis and luminescent properties of Dy³⁺-doped La₂Sn₂O₇ nanocrystals [J]. *Materials Science and Engineering B*, 2007, 143(1–3): 90–93.
- [12] MOON J, AWANO M, MAEDA K. Hydrothermal synthesis and formation mechanisms of lanthanum tin pyrochlore oxide [J]. *Journal of the American Ceramic Society*, 2001, 84(11): 2531–2536.
- [13] MAO Ya-chun, LI Guang-she, XU Wei, FENG Shou-hua. Hydrothermal synthesis and characterization of nanocrystalline pyrochlore oxides M₂Sn₂O₇ (M=La, Bi, Gd or Y) [J]. *Journal of Materials Chemistry*, 2000, 10(2): 479–482.
- [14] DING Gao-song, ZHU Lu-ming, YANG Hong, YU Gui-xia, ZHU Hong-liang, YAO Kui-hong. Hydrothermal synthesis and characterization of flake-like lanthanum stannate nanostructures [J]. *Journal of Zhejiang Sci-Tech University*, 2007, 24(5): 557–561. (in Chinese).
- [15] SPEIGHT J. Lange's handbook of chemistry [M]. New York: McGraw-Hill, 2005.
- [16] LI Hai-bin, LIU Guo-cong, DUAN Xue-chen. Monoclinic BiVO₄ with regular morphologies: Hydrothermal synthesis, characterization and photocatalytic properties [J]. *Materials Chemistry and Physics*, 2009, 115(1): 9–13.
- [17] XU Shu-ling, SONG Xin-yu, FAN Chun-hua, CHEN Guo-zhu, ZHAO Wei, YOU Ting, SUN Si-xiu. Kinetically controlled synthesis of Cu₂O microcrystals with various morphologies by adjusting pH value [J]. *Journal of Crystal Growth*, 2007, 305(1): 3–7.
- [18] DJERDJ I, GARNWEITNER G, SU D S, NIEDERBERGER M. Morphology-controlled nonaqueous synthesis of anisotropic lanthanum hydroxide nanoparticles [J]. *Journal of Solid State Chemistry*, 2007, 180(7): 2154–2165.
- [19] REN Yang, MA Jun-feng, WANG Yong-gang, ZHU Xiao-yi, LIN Bo-tao, LIU Jun, JIANG Xiao-hui, TAO Jian-tao. Shape-tailored hydrothermal synthesis of CdMoO₄ crystallites on varying pH conditions [J]. *Journal of the American Ceramic Society*, 2007, 90(4): 1251–1254.
- [20] GUPTA H C, BROWN S, RANI N, GOHEL V B. A lattice dynamical investigation of the Raman and the infrared frequencies of the cubic A₂Sn₂O₇ pyrochlores [J]. *International Journal of Inorganic Materials*, 2001, 3(7): 983–986.
- [21] ZHANG F X, MANOUN B, SAXENA S K, ZHA C S. Structure change of pyrochlore Sm₂Ti₂O₇ at high pressures [J]. *Applied Physics Letters*, 2005, 86(18): 181906.
- [22] GARG N, PANDEY K K, MURLI C, SHANAVAS K V, MANDAL B P, TYAGI A K, SHARMA S M. Decomposition of lanthanum hafnate at high pressures [J]. *Physical Review B*, 2008, 77(21): 214105.
- [23] FUENTES A F, BOULALLYA K, MACZKA M, HANUZA J, AMADOR U. Synthesis of disordered pyrochlores, A₂Ti₂O₇ (A=Y, Gd and Dy), by mechanical milling of constituent oxides [J]. *Solid State Sciences*, 2005, 7(4): 343–353.
- [24] LI Yan-ping, ZHANG Jian-hua, ZHANG Xia, LUO Yong-shi, LU Shao-zhe, REN Xin-gang, WANG Xiao-jun, SUN Ling-dong, YAN Chun-hua. Luminescent properties in relation to controllable phase and morphology of LuBO₃:Eu³⁺ nano/microcrystals synthesized by hydrothermal approach [J]. *Chemistry of Materials*, 2009, 21(3): 468–475.
- [25] TABOR C, MURALI R, MAHMOUD M, EL-SAYED M A. On the use of plasmonic nanoparticle pairs as a plasmon ruler: The

- dependence of the near-field dipole plasmon coupling on nanoparticle size and shape [J]. *Journal of Physical Chemistry A*, 2008, 113(10): 1946–1953.
- [26] HUANG Yan, YE Hong-qi, ZHUANG Wei-dong, HU Yun-sheng, ZHAO Chun-lei, LI Cui, GUO Song-xia. Preparation of $Y_2O_3:Eu^{3+}$ phosphor by molten salt assisted method [J]. *Transactions of Nonferrous Metals Society of China*, 2007, 17(3): 644–648.
- [27] SRIVASTAVA A M. Chemical bonding and crystal field splitting of the $Eu^{3+} \ ^7F_1$ level in the pyrochlores $Ln_2B_2O_7$ ($Ln=La^{3+}, Gd^{3+}, Y^{3+}, Lu^{3+}, B=Sn^{4+}, Ti^{4+}$) [J]. *Optical Materials*, 2009, 31(6): 881–885.
- [28] ZHANG Ming, LI Xin-hai, WANG Zhi-xing, HU Qi-yang, GUO Hua-jun. Synthesis of $Y_2O_3:Eu^{3+}$ phosphors by surface diffusion and their photoluminescence properties [J]. *Transactions of Nonferrous Metals Society of China*, 2010, 20(1): 115–118.
- [29] CHEN Di, SHEN Guo-zhen, TANG Kai-bin, LIANG Zhen-hua, ZHENG Hua-gui. AOT-microemulsions-based formation and evolution of $PbWO_4$ crystals [J]. *Journal of Physical Chemistry B*, 2004, 108(31): 11280–11284.
- [30] JOSEPH L K, DAYAS K R, DAMODAR S, KRISHNAN B, KRISHNANKUTTY K, NAMPOORI V P N, RADHAKRISHNAN R. Photoluminescence studies on rare earth titanates prepared by self-propagating high temperature synthesis method [J]. *Spectrochimica Acta Part A*, 2008, 71(4): 1281–1285.
- [31] LIU Guo-cong, DUAN Xue-chen, LI Hai-bin, DONG Hui. Hydrothermal synthesis, characterization and optical properties of novel fishbone-like $LaVO_4:Eu^{3+}$ nanocrystals [J]. *Materials Chemistry and Physics*, 2009, 115(1): 165–171.

八面体状 $La_2Sn_2O_7:Eu^{3+}$ 微晶的水热合成、表征与光学性能

杨锦瑜^{1,2}, 苏玉长¹, 刘雪颖^{1,3}

1. 中南大学 材料科学与工程学院, 长沙 410083;
2. 贵州师范大学 化学与材料科学学院, 贵阳 550001;
3. 广西工学院 科技处, 柳州 545006

摘要: 采用水热法在 180 °C 下反应 36 h 合成了具有规整八面体状的烧绿石结构 $La_2Sn_2O_7:Eu^{3+}$ 微晶。采用 XRD、TEM、SEM、EDS、FT-IR、Raman 和 PL 对合成产物的晶体结构、颗粒尺寸、形貌和光学性能进行了研究。对前驱体溶液的 pH 值、前驱体浓度、水热反应温度和水热反应时间等工艺条件的影响进行了研究。研究结果证实前驱体溶液的 pH 值不仅决定合成产物的物相结构, 而且对合成产物的形貌也具有显著的影响。在 pH 值为 12 时可以获得平均尺寸为 700 nm 的规整八面体状晶体。提出了八面体状 $La_2Sn_2O_7:Eu^{3+}$ 微晶的可能形成机理。光致发光光谱显示: 八面体状 $La_2Sn_2O_7:Eu^{3+}$ 微晶与其它形貌的样品相比较, 在 582–592 nm 区域具有更强的发光强度。

关键词: 烧绿石结构; 水热合成; 生长机理; 光学性能

(Edited by YANG Hua)